

Phase diagram of sustained wave fronts opposing the flow in disordered porous media

SANDEEP SAHA, SEVERINE ATIS, DOMINIQUE SALIN and LAURENT TALON

UPMC Univ Paris 06, Univ. Paris-Sud, CNRS, Lab. FAST - Bât. 502, Campus Univ., Orsay, F-91405, France, EU

received 23 October 2012; accepted in final form 15 January 2013
published online 13 February 2013

PACS 82.40.Ck – Pattern formation in reactions with diffusion, flow and heat transfer
PACS 47.54.-r – Pattern selection; pattern formation
PACS 82.33.Ln – Reactions in sol gels, aerogels, porous media

Abstract – Using lattice Boltzmann simulations, we analyze the different regimes of propagation of an autocatalytic reaction front in heterogenous porous media. The heterogeneities of the porous medium are characterized by the standard deviation of its log-normal distribution of permeability and its correlation length. We focus on the situation where chemical reaction and flow field act in opposite directions. In agreement with previous experiments we observe upstream, downstream fronts as well as static, frozen ones over a range of flow velocity which depends drastically on the heterogeneities of the flow field. The transition between the static regime and the downstream one account for large enough low-velocity zones, whereas the transition from static to upstream regime is found to be given by a kind of percolation path.

 Copyright © EPLA, 2013

Introduction. – Reactive front propagations are relevant to a wide range of dynamical systems such as population balance [1,2], chemical reactions [3], plasma physics [4], epidemics [5], and chemotaxis [6] to mention a few of them. The dynamics of autocatalytic chemical reactions in stagnant fluids is now well understood [1–3]: the front propagates at a constant velocity V_χ with a width l_χ resulting from a balance between molecular diffusion and reaction rate. In the present paper, we are interested in third-order autocatalytic reactions which can be described by an advection-reaction-diffusion equation for the concentration c of the reactants,

$$\frac{\partial c}{\partial t} + \vec{\nabla} \cdot (c \vec{U}) = D_0 \Delta c + \alpha c^2 (1 - c), \quad (1)$$

where the mixed second-third order kinetics corresponds to the iodate-arsenous acid reaction used in the corresponding experiments [3,7,8]; D_0 is the molecular diffusion coefficient, α the reaction rate and \vec{U} is the flow velocity. In the absence of flow, the front thickness reaches a constant finite value $l_\chi = \sqrt{2D_0/\alpha}$ and a chemical wave velocity $V_\chi = \sqrt{D_0\alpha/2}$.

Such propagation in simple flows has been addressed recently [7,9]. In more complex situations from the point of view of either the chemistry [10,11] or the flow field [8,12–14], it has been reported that when the flow

is opposing the chemical front, frozen, *i.e.*, static, fronts can be observed not only for a particular flow intensity, but also over a wide range of flow intensity values. Those frozen states have been observed experimentally but not fully understood. Hereby, we analyse those states in the light of numerical simulations and a model porous medium which offer the main advantage of controllability of the velocity field. We analyze the different regimes of propagation of an autocatalytic reaction front in heterogenous porous media. We model these heterogeneities, using a log-normal distribution of permeability (*i.e.*, flow resistance) of standard deviation, σ and correlation length, λ [15,16]. These two parameters control the heterogeneities of the flow field in the porous medium, another important parameter is of course the adverse flow intensity \bar{U} which must be compared to the reaction which propagates at the velocity V_χ . We will demonstrate later that the chemical length l_χ is also a relevant parameter. In the simulations we do observe behaviors analogous to those in the experiments [8,14], the front propagating upstream, downstream and especially the static state over a wide range of \bar{U} . We analyze the dependence of the range of static fronts with σ and λ . These “frozen states” can be understood as the consequence of the flow field heterogeneities. An algorithm, based on percolation theory, is developed to predict the boundaries of this static regime in the parameter space.

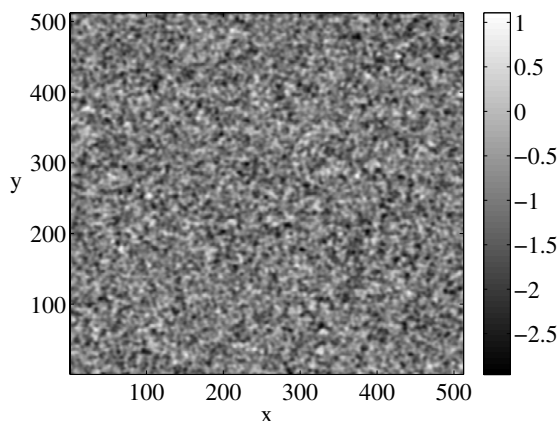


Fig. 1: Stochastically generated permeability field.

Porous medium and chemical numerical simulations. – Figure 1 shows a typical permeability field used in our simulations [16]. The heterogeneous porous medium was stochastically generated with a permeability field distribution following a correlated log-normal distribution [17]. Therefore, the probability distribution function (PDF) of the permeability logarithm, $f = \ln(K)$ reads as follows:

$$\text{PDF}(f) \propto \exp\left(-\frac{(f - f_0)^2}{2\sigma_f^2}\right), \quad (2)$$

$$\hat{f}\hat{f}^*(\vec{k}) = \frac{2\sigma_f^2}{\pi k_0^2} \exp\left(-2\frac{|k|^2}{k_0^2}\right), \quad (3)$$

where $\hat{\cdot}$ refers to the Fourier transform and \cdot^* the complex conjugate. The heterogeneities of the porous media are characterized by the harmonic mean permeability $K_0 = \exp(f_0)$, the standard deviation σ_f and the correlation length $\lambda = \pi/k_0$. A pressure gradient, applied along the x -direction, generates a flow field of mean velocity \bar{U} . The chemical reaction is initiated ($t = 0$) at a location x_0 with reactants on the left and products on the right. The flow field and the reaction diffusion equation were solved using the lattice Boltzmann method (for general references, see [18–20], for reaction diffusion systems [21–23]). The methods have been successfully applied for flow in heterogeneous porous media and reactive transport (*e.g.*, [16,24–27]). The simulations are performed in two steps: First, we solve the flow transport by solving the Darcy-Brinkman equation. Once the flow has reached its steady state, the chemical reaction propagation is then simulated. In the following we analyze the case of flow adverse to the chemical reaction; we normalize all the velocities by the chemical wave velocity V_χ and the lengths by l_χ ; as \bar{U} is negative compared to V_χ , we use $u = -\bar{U}/V_\chi$ as the flow intensity control parameter. In the simulations, it is observed that the reaction front travels at a constant velocity, V_f , either downstream, upstream or remains static depending on u ; hence $v_f = V_f/V_\chi$ is either negative, null or positive, respectively. We also

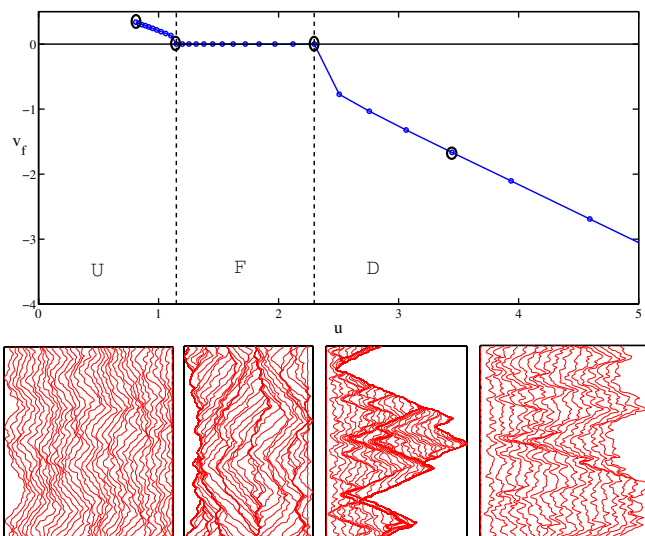


Fig. 2: (Colour on-line) Front velocity $v_f = V_f/V_\chi$ vs. average flow velocity $u = -\bar{U}/V_\chi$ revealing the different regimes: U and D correspond, respectively, to a regime of front propagation upstream and downstream, whereas the plateau corresponds to static, *i.e.*, frozen, fronts (F). $\sigma = 0.5$ and $l_\chi/\lambda = 0.126$. $\sigma = 0.5$ and $l_\chi/\lambda = 0.126$. The bottom figures shows the evolution of the reaction front every 20000 time steps in each regime (corresponding to the encircled points from left to right in the same order).

note that a resolution check has been performed, which leads to an error smaller than ten percent.

Results. – Figure 2 shows the variation of the reaction front velocity v_f vs. the mean adverse flow velocity u for $\sigma = 0.5$ and $l_\chi/\lambda = 0.126$. We observe three different regimes: For low velocities (regime U), the front travels upstream, that is in the same direction as that of the chemical reaction ($v_f > 0$). For a range of velocities (regime F), the front becomes static ($v_f = 0$): this the “frozen state” plateau mentioned before. At higher velocities (regime D), the front travels downstream ($v_f < 0$). These regimes, as well as the typical front shapes (fig. 2), are in agreement with the experiments [8]. Interestingly, the static regime also displays the very characteristic “V-shaped” structure observed in experiments [8]. The agreement between experiments and our model porous medium reveals that introducing heterogeneities allows one to reproduce the static “frozen states” plateau observed experimentally, even though the velocity distribution and correlation are different. One of the goals of this paper is to understand the occurrence of the static state and the plateau’s extent. Figure 3 presents the variation of v_f vs. u with each of the two control parameters of the heterogeneities, l_χ/λ and σ , while keeping the other one constant. Figure 3(a) shows that increasing l_χ/λ while keeping σ constant reduces the plateau width; moreover, this reduction occurs mainly on the side of the $F \leftrightarrow D$ (FD) transition, whereas the $U \leftrightarrow F$ (UF) transition corresponds always to the

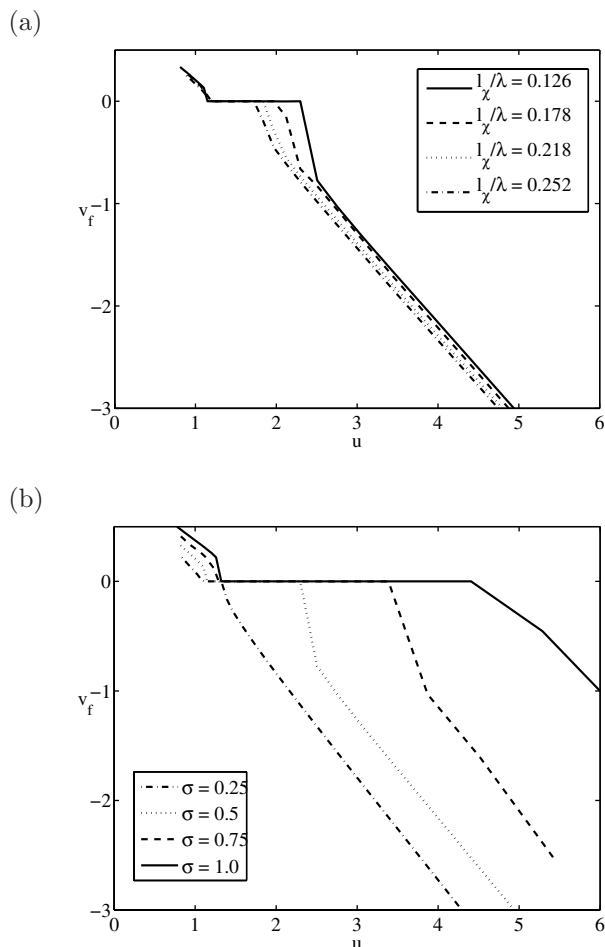


Fig. 3: Variation of the width of the plateau region as a function of the two heterogeneity parameters, l_x/λ and σ . (a) v_f vs. u for different l_x/λ keeping $\sigma = 0.5$ constant. (b) v_f vs. u for different σ keeping $l_x/\lambda = 0.126$ constant.

same u value. Keeping l_x/λ constant and increasing the amplitude of heterogeneities (*i.e.*, σ , fig. 3(b)), increases significantly the width of the plateau region. The FD transition is clearly more affected while the UF transition remains unaffected. As σ tends to zero, that is a homogeneous porous medium, the plateau region vanishes and the velocity variation tends towards the linear law, $v_f \approx 1 - u$, ($V_f = \bar{U} + V_\chi$) which is the expected behavior for a homogenous flow field leading to a simple Galilean sum rule [7,9]; in this case the front is static only for a single flow value ($u = 1$). To summarize these features, fig. 4 represents the phase diagram of the different regimes as a function of the two heterogeneity parameters, l_x/λ and σ .

Discussion. – In order to account for zero-velocity fronts in porous media, refs. [10,11] emphasize the influence of “excited stagnant pockets” that would act as point source accounting for pinning the front spatially. This assertion needs, however, to be completed: in our numerical porous medium, we do observe static fronts

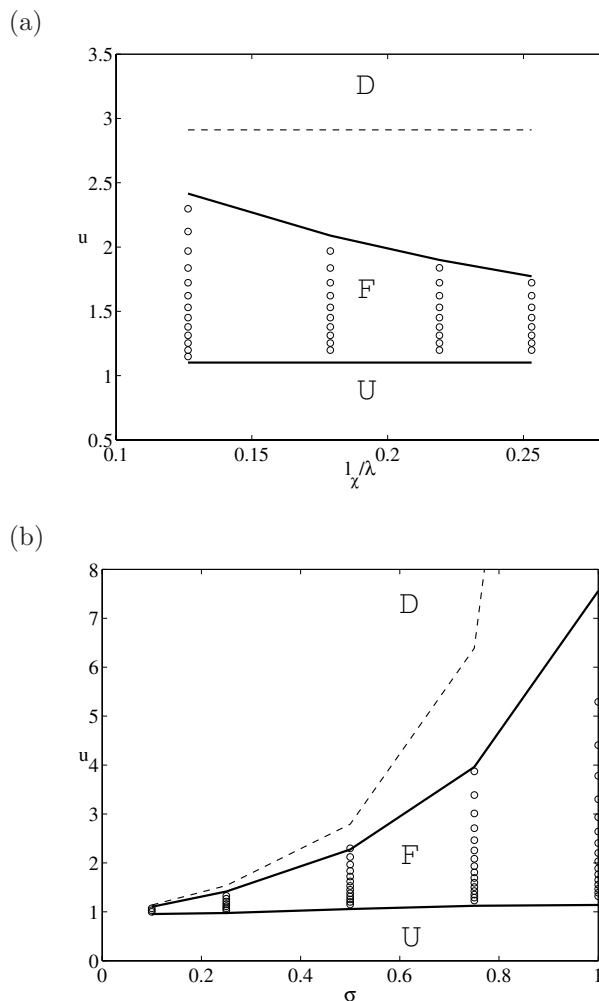


Fig. 4: Diagram of the observed regimes (U , F , D). The circles corresponds to observation of frozen fronts (F : $v_f = 0$), hence the vertical give the u variation of the frozen state plateau. (a) u vs. l_x/λ at constant $\sigma = 0.5$. (b) u vs. σ for $l_x/\lambda = 0.126$. The thin dashed lines correspond to the first rough estimate of the FD transition using eq. (4), whereas the thick solid bold lines correspond to a more refined one (eq. (5)). The bottom bold, almost straight, lines in both figures correspond to the percolation like prediction of the UF transition (see text).

although we do not have any stagnant zones. In addition, this mechanism did not explain why, for sufficiently large velocities, the front is pushed back again. Indeed the phenomenon has only been observed previously for different complex chemical reaction in combined cellular flow and mean flow [13] where stagnation points are scarce. Such a plateau was observed recently experimentally in packed beads [8,14]. As we do not have stagnation points but only low-velocity zones to account for the plateau, we display in fig. 5 the velocity fields and front shapes for different regimes. To identify the low-velocity zones, we have drawn in white the iso-velocity contours corresponding to $U(x, y) = -V_\chi$. From top to bottom (D to U regimes), u decreases and the number and the extension of white lines increase. Let us first address the FD

transition. It is likely that the main difference between regime D and regime F (the two top figures of fig. 5) is the presence of numerous white spots in the frozen regime where locally the mean flow is lower than the chemical velocity. We observe that the front gets pinned in these zones. Inside these spots the catalysis concentration has reached unity and act as a source point or zone for its neighbors. This can also explain the V-shape structure (fig. 2) which is the solution of the source point inside an uniform adverse flow [8].

These observation lead to a first estimate of the transition velocity u_{FD} between frozen and downstream regimes,

$$\min(U(x, y)) = -V_\chi. \quad (4)$$

In other words, the transition occurs when the chemical velocity becomes smaller than the global minimum of the velocity field. This criterion has been plotted on the phase diagram in fig. 4 as the thin dashed line which indeed is a larger bound that over predicts the transition and does not account for the effect of l_χ/λ . The relevance of this latter ratio can be addressed in the context of eikonal [28] and mixing regimes [9,29]. In the mixing regime, the front width is much larger than the characteristic length scale of the flow which in this problem is the correlation length of the permeability field λ ; in this case the chemical front is sensitive to the average velocity over the distance l_χ and therefore feels the average velocity field \bar{U} and behaves like in the homogeneous medium leading to the above disappearance of the plateau. In the opposite case, the so-called eikonal (thin-front) regime, the front width is much smaller than any length scale in the system and, therefore, is sensitive to local velocities. Indeed, in our simulation we are in between these two regimes but the global trend is in agreement with the above discussion (decreasing l_χ/λ leads to a shorter plateau); therefore, the finite width l_χ has to be taken into account in the pinning criteria. We can expect that the lower-velocity zones influence the dynamics of the front when they have a sufficiently large extension: in fig. 5(b), we note that the front has passed through low-velocity zones before being pinned. Following the determination of the contours of all the low-velocity zones, we compute the width l_{FD} of each of them, and retain those with a large enough size:

$$l_{FD} \geq 9l_\chi, \quad (5)$$

where the numerical factor (9) is an *ad hoc* coefficient that best fits the transition. The corresponding criterion is represented in fig. 4 (thick dashed line) and shows reasonable agreement for the variations of both parameters.

Increasing σ or increasing λ/l_χ naturally increase the probability to pin the front. Even if the variation with the disorder of the transition velocity $U \leftrightarrow F$ is not very large, figs. 5(c), (d) give some insight into the physical mechanism at work. As u is decreased, the number and the size of weak-velocity zones increase. In these regions, where

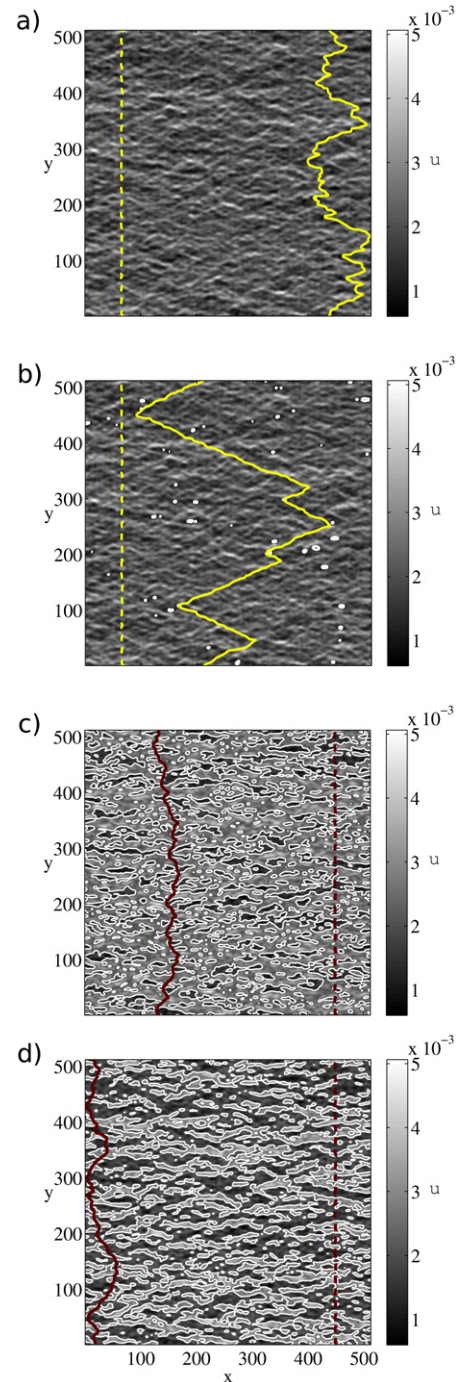


Fig. 5: (Colour on-line) In grey scale, velocity field. White lines correspond to the velocity iso-contours $U(x, y) = -V_\chi$, where $U(x, y)$ is the local velocity. From top to bottom: (a) downstream regime (D , $u = 4$); (b) frozen regime (F , $u = 3$) close to the FD transition; (c) frozen regime (F , $u = 1.5$) but close to the UF transition; and (d) upstream regime (U , $u = 0.8$). Fluid is flowing from left to right, whereas the chemical wave in the absence of flow would propagate from right to left. In each figure, the vertical, almost straight line corresponds to the initial front position; the jagged lines correspond to the frozen front for the F regime, and to its location in the ultimate frame before the front leaves the medium at the right (D regime) and at the left (U regime).

the flow is weaker, the front can in principle propagate upstream and then stop only when it reaches the left-end side of these zones. Consequently, we can reasonably think that one condition for the front to travel upstream is that it found a path connecting the initial front position to the left-end side of the system where the flow is weaker than the chemical reaction. This is reminiscent of percolation-like approaches. Therefore, the UF transition is likely to be determined by a path criterion which is found using the min-max algorithm described by [30]. For all the paths \mathcal{C} connecting the left-end side of the domain to the initial position of the front, we compute the maximal velocity. At the transition, the chemical velocity V_χ has then to be equal to the minimum of those maxima,

$$U_{perc} = \min_{\mathcal{C}} \left(\max_{(x,y) \in \mathcal{C}} U(x,y) \right).$$

For directed percolation, this velocity can be determined recurrently. We can describe briefly the sequences used for this determination. It consists of introducing a matrix $C_{i,j}$ defined as the minimum of the maximal velocity found on all paths connecting the first column to point (i,j) :

- 1) Initialize the first column of the matrix, $C_{1,j}$ which consists of the velocity field at the inlet (i,j correspond to the x,y coordinates, respectively).
- 2) At the next downstream location, (i) , we find $C_{min}(i,j) \equiv \min\{C_{i,j-1}, C_{i,j}, C_{i,j+1}\}$ for all (j) .
- 3) Then we assign $C_{i+1,j} = \max\{C_{min}(i,j), u_{i+1,j}\}$.
- 4) Repeat steps 2 and 3 until the other side of the domain opposite to the inlet is reached.
- 5) $u_{perc} = \min\{C(N_x, [1, 2, 3 \dots N_y])\}$ where N_x, N_y are the number of points in the x,y direction, respectively.

The percolation path is then found by following the reverse algorithm. Figure 6 shows the percolation path corresponding to the percolation velocity for the velocity field corresponding to fig. 1. Using the aforementioned algorithm we compute U_{perc} and compare it to the observed UF transition for various values of l_χ and σ in figs. 4(a), (b) marked by the bottom solid bold lines. The percolation velocity gives an accurate estimate of the critical velocity for the transition from the upstream regime to the frozen regime, even though the variations with either parameter is small; since the percolation threshold on a regular lattice is close to $1/2$, the percolation velocity satisfies $\int_{-\infty}^{u_c} \text{PDF}(u) du \simeq 1/2$. It is thus expected that the critical chemical velocity would be close to the mean flow velocity if the probability distribution were symmetrical. Moreover, we expect that the amplitude of the heterogeneities and their correlation have very little influence on the critical velocity which is confirmed by fig. 4. One should however recall that our flow velocity field has a log-normal distribution and has anisotropy, which could explain that percolation is occurring for $u > 1$ and is sensitive to σ .

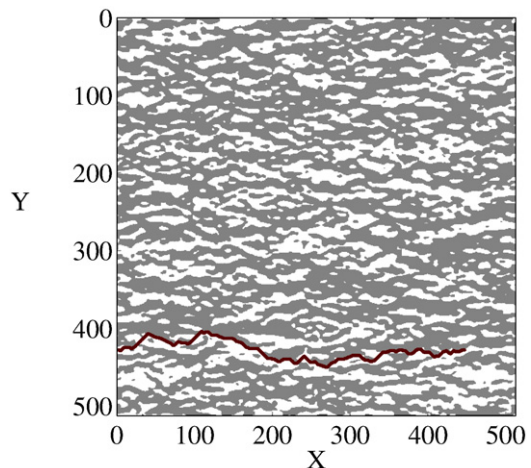


Fig. 6: (Colour on-line) Percolation path. White and black regions correspond, respectively, to $U(x,y) < u_c$ and $U(x,y) > u_c$.

One notes in fig. 6 that, close to percolation, higher-velocity regions are also percolating to the right-end side. The front is however propagating upstream because of the autocatalytic process. Wherever the reaction manages to propagate upstream, it acts as a source of catalysis from that point and can then excite neighbouring area. The upstream propagation has therefore an ascendent on the downstream one. In addition, one can note that the front is going upstream slightly before percolation. This can be explained also by the autocatalytic process: due to the fact that an “excited” low-velocity cluster can excite other neighboring clusters that might span further upstream. Non-percolating clusters might then be excited further and further upstream. Note that the finite width of the chemical front, in which case, a cluster can excite the other if the distance between the two is smaller than the chemical length.

Conclusions. – Using lattice Boltzmann simulations, we have modeled and analyzed the different regimes of propagation of an autocatalytic reaction front in heterogeneous porous media when chemical reaction and flow field act in opposite directions. In agreement with previous experiments on a packed-beads porous medium, we observe upstream, downstream fronts as well as static, frozen ones over a range of flow velocity which depends drastically on the heterogeneities of the flow field. The transition between the static regime and the downstream one is due the presence of large enough low-velocity zones, whereas the transition from the static to the upstream regime is found to be given by a kind of percolation path.

REFERENCES

- [1] FISHER R., *Ann. Eugen.*, **7** (1937) 355.
- [2] KOLMOGROFF A., PETROVSKY I. and PISCOUNOFF N., *Bull. Univ. d’État à Moscou*, **1** (1937) 1.

- [3] SCOTT S. K., *Oscillations, Waves, and Chaos in Chemical Kinetics* (Oxford University Press) 1994.
- [4] BEULE D., FÖRSTER A. and FRICKE T., *Z. Phys. Chem.*, **204** (1998) 1.
- [5] RUSSELL C., SMITH D., WALLER L., CHILDS J. and REAL L., *Proc. R. Soc. London, Ser. B*, **271** (2004) 21.
- [6] ADLER J., *Science*, **153** (1966) 708.
- [7] LECONTE M., MARTIN J., RAKOTOMALALA N. and SALIN D., *Phys. Rev. Lett.*, **90** (2003) 128302.
- [8] ATIS S., AURADOU S. S. H., TALON L. and SALIN D., <http://arxiv.org/abs/1210.3518> (2012).
- [9] EDWARDS B. F., *Phys. Rev. Lett.*, **89** (2002) 104501.
- [10] KAERN M. and MENZINGER M., *J. Phys. Chem. B*, **106** (2002) 3751.
- [11] KOPTYUG I. V., ZHIVONITKO V. V. and SAGDEEV R. Z., *J. Phys. Chem. B*, **112** (2008) 1170.
- [12] PAOLETTI M. S. and SOLOMON T. H., *Europhys. Lett.*, **69** (2005) 819.
- [13] SCHWARTZ M. E. and SOLOMON T. H., *Phys. Rev. Lett.*, **100** (2008) 028302.
- [14] ATIS S., SAHA S., AURADOU H., MARTIN J., RAKOTOMALALA N., TALON L. and SALIN D., *Chaos*, **22** (2012) 037108.
- [15] MATHERON G., *Eléments pour une théorie des milieux poreux* (Masson, Paris) 1967.
- [16] TALON L., MARTIN J., RAKOTOMALALA N., SALIN D. and YORTSOS Y., *Water Resour. Res.*, **39** (2003) 1135.
- [17] GELHAR L. and AXNESS C., *Water Resour. Res.*, **19** (1983) 161.
- [18] SUCCI S., FOTI E. and HIGUERA F., *Europhys. Lett.*, **10** (1989) 433.
- [19] QIAN Y., D'HUMIÈRES D. and LALLEMAND P., *Europhys. Lett.*, **17** (1992) 479.
- [20] BENZI R., SUCCI S. and VERGASSOLA M., *Phys. Rep.*, **222** (1992) 145.
- [21] DAWSON S. P., CHEN S. and DOOLEN G. D., *J. Chem. Phys.*, **98** (1993) 1514.
- [22] SUCCI S., GABRIELLI A., SMITH G. and KAXIRAS E., *Eur. Phys. J. Appl. Phys.*, **16** 71.
- [23] GINZBURG I., D'HUMIÈRES D. and KUZMIN A., *J. Stat. Phys.*, **139** (2010) 1090, 10.1007/s10955-010-9969-9.
- [24] TALON L., MARTIN J., RAKOTOMALALA N. and SALIN D., *Phys. Fluids*, **16** (2004) 4408.
- [25] LECONTE M., JARRIGE N., MARTIN J., RAKOTOMALALA N., SALIN D. and TALON L., *Phys. Fluids*, **20** (2008) 057102.
- [26] JARRIGE N., BOU MALHAM I., MARTIN J., RAKOTOMALALA N., SALIN D. and TALON L., *Phys. Rev. E*, **81** (2010) 066311.
- [27] TALON L., AURADOU H. and HANSEN A., *EPL*, **97** (2012) 68009.
- [28] WILLIAMS F., *Combustion Theory*, 2nd edition (Benjamin/Cummings) 1985.
- [29] LECONTE M., MARTIN J., RAKOTOMALALA N. and SALIN D., *J. Chem. Phys.*, **120** (2004) 7314.
- [30] HANSEN A. and ROUX S., *J. Phys. A: Math. Gen.*, **20** (1987) L873.